Ultrasound in Med. & Biol., Vol. 38, No. 11, pp. 1958–1969, 2012

0301-5629/$ - see front matter

http://dx.doi.org/10.1016/j.ultrasmedbio.2012.07.009

● *Original Contribution*

BIOEFFECTS OF ULTRASOUND-STIMULATED MICROBUBBLES ON ENDOTHELIAL CELLS: GENE EXPRESSION CHANGES ASSOCIATED WITH RADIATION ENHANCEMENT *IN VITRO*

Azza A. Al-Mahrouki,*†‡ Raffi Karshafian,§ Anoja Giles,*†‡ and Gregory J. Czarnota*†‡

*Radiation Oncology and Imaging Research, Sunnybrook Health Sciences Centre, Toronto, Ontario, Canada; †Department of Radiation Oncology, Faculty of Medicine, University of Toronto, Toronto, Ontario, Canada; ‡Department of Medical Biophysics, Faculty of Medicine, University of Toronto, Toronto, Ontario, Canada; and §Department of Physics, Ryerson University, Toronto, Ontario, Canada

(*Received* 19 *December* 2011; *revised* 6 *June* 2012; *in final form* 16 *July* 2012)

Abstract—Ultrasound can be used to target endothelial cells in cancer therapy where the destruction of vasculature leads to tumor cell death. Here, we demonstrate ultrasound bioeffects in which the levels of genes in endothelial cells can be significantly altered by ultrasound-stimulated microbubble exposure. These were compared with established effects of radiation on endothelial cells at a gene level. Human-endothelial cells were exposed to ultrasound and microbubbles, radiation or combinations of ultrasound, microbubbles and radiation. Gene expression analyses revealed an up-regulation of genes known to be involved in apoptosis and ceramide-induced apoptotic pathways, including *SMPD2*, *UGT8*, *COX6B1*, *Caspase 9* and *MAP2K1* with ultrasound-stimulated microbubble exposure but not *SMPD1*. This was supported by immunohistochemistry and morphologic changes examined with cell microscopy, which showed changes in *SMPD1* gene product in cells with microbubble exposure. This supports the hypothesis that ultrasound-stimulated microbubbles can induce significant bioeffect-related changes in gene expression and can affect ceramide signaling pathways in endothelial cells, leading to apoptosis. (E-mail: Gregory.Czarnota@sunnybrook.ca)

Key Words: **Ultrasound, Microbubbles, Radiation, Gene expression, Ceramide, Apoptosis, Bioeffect.**

INTRODUCTION

Ultrasound methods are increasingly being used to image biomarkers on endothelial cells (Hu et al. 2011), and for therapy they target endothelial cells in a number of different manners that range from bioeffects such as transient sonoporation to more disruptive methods (Liao et al. 2012; O'Reilly et al. 2010). Endothelial cells play an important role in blood vessel development and maturation. This is important in the process of angiogenesis (Suchting and Eichmann 2009), which can be induced in response to the lack of oxygen (hypoxia) in tumors (Hanahan and Folkman 1996). Anti-angiogenic drugs, which mainly target vascular endothelial growth factor (VEGF), have been considered to be effective as treatment agents in cancer therapy but only typically result in transient blocks to tumor growth (Bergers and Hanahan 2008). Targeting VEGF can partially induce apoptosis in endothelial cells, leading to the degeneration of blood vessels. Nevertheless, the use of anti-VEGF agents in clinical trials has not yet directly supported this hypothesis (Ellis and Hicklin 2008a). There may be numerous reasons contributing to the apparent clinical lack of effectiveness of anti-angiogenic drugs. These include characteristically abnormal leaky blood vessels in tumors, which can contribute to hypoxia and continuously promote the formation of new vessels (Bautch 2009) or can be related to the diverse mechanisms of actions of these drugs that follow various pathways, which can lead to the development of resistance. Even when combining anti-VEGF drugs with chemotherapy, resistance to treatment has been observed (Ellis and Hicklin 2008b). Chemical vascular disrupting agents work very well to cause endothelial cell death and vessel collapse, leading to rapid tumour necrosis. However, this treatment also stimulates aggressive regrowth from the

Address correspondence to: Gregory J. Czarnota, Ph.D., M.D., Radiation Oncologist and Clinician Scientist, Departments of Radiation Oncology and Imaging Research, Sunnybrook Health Sciences Centre Assistant Professor, Departments of Radiation Oncology and Medical Biophysics, University of Toronto, 2075 Bayview Ave, T2-167, Toronto, ON M4N 3M5. E-mail: Gregory.Czarnota@sunnybrook.ca

surviving viable cell vascularized rim (Tozer et al. 2005). This has increased the need to develop a novel therapeutic approach to target tumor angiogenesis more effectively.

Chemical cues in addition to mechanical factors are known to contribute to the regulation of neovascularization and may interact to control vascular growth (Mammoto et al. 2009). The chemical disturbance of endothelial cells, in addition to mechanical perturbation, can thus potentially interfere with vascular integrity, which is essential for tumor cell survival. Tumor cell death in the case of such vascular perturbation can be secondary to endothelial cell death, as previously demonstrated in responses to radiotherapy (GarciaBarros et al. 2003). There have been recent demonstrations of novel uses of microbubbles stimulated by ultrasound as a new anticancer therapy used alone (Wood et al. 2008), with chemotherapy (Sorace et al. 2012) or in combination with radiotherapy (Czarnota et al., 2012; Tran et al., 2012).

Microbubbles are micron-size, gas-filled, lipid-encapsulated agents typically used as imaging contrast agents. For imaging purposes, microbubble-disruption-replenishment experiments have recently been used to characterize blood flow within tissues and tumors (Gerst et al. 2011; Hoyt et al. 2011; Olson et al. 2011). Most recently, these have been used to create parametric maps of tissue or tumor perfusion (French et al. 2006). The disruptions, thought to be clinically benign, have previously been associated with biologic effects such as premature ventricular contractions when used for cardiac imaging (Rota et al. 2006; Tran et al. 2009) and recently with blood vessel damage under imaging conditions (McDannold et al. 2011).

For the purposes of therapy, in the presence of ultrasound, microbubbles can also be induced to resonate and be burst, thus transferring mechanical energy to nearby cellular membranes. Microbubbles have been recently used in therapeutic applications ranging from sonothrombolysis (Alonso et al. 2009; Brown et al. 2011) to lowering the heating threshold for high-intensity focused ultrasound (McDannold et al. 2006; Klotz et al. 2010) and to facilitate drug and gene delivery through sonoporation (Karshafian et al. 2010; Liao et al. 2011). In the latter application, the use of ultrasound in the presence of microbubbles has been demonstrated to improve intracellular delivery of therapeutic molecules by increasing the permeability of plasma cell membranes. In addition, similar methods are being investigated for transient blood-brain-barrier disruption (Chopra et al. 2010; Jalali et al. 2010; O'Reilly et al. 2010).

Recent experiments combining the ultrasound-stimulated microbubble treatments with radiation have demonstrated a synergistic effect with a 50–70% tumor volume ablation when used combination with single radiation doses (Czarnota et al., 2012; Tran et al., 2012). The mechanism of vascular disruption in those experiments has been determined to be potentially endothelial cell apoptosis.

Apoptosis in endothelial cells secondary to radiation has been reported to be associated with sphingomyelinases (GarciaBarros et al. 2003), which are known to use sphingomyelin as a substrate to produce ceramide. A second messenger, ceramide, can lead to apoptosis (Barnes 2004) through the activation of a well-known apoptotic pathway that leads to the activation of caspases, eventually causing cell death. In addition, *de novo* synthesis of ceramide is also known to be involved in the regulation of *caspase 9* in lung adenocarcinoma cells (Chalfant et al. 2002). Ceramide is also known to be associated with cell stressors including septic shock, ischemia reperfusion, various chemotherapy agents, heat stress and radiation effects (Nikolova-Karakashian and Rozenova 2010).

The objective of this study was to investigate and identify a potential signaling pathway that regulates apoptosis in endothelial cells in response to ultrasound-microbubble anticancer treatments. We have characterized the up-regulation of a number of genes, using microarray analysis and real-time polymerase chain reaction (RT-PCR), which code for peptides that are possibly involved in microbubble-induced cell membrane damage and ceramide-activated apoptosis. These genes included those coding for *sphingomyelinase* (*SMPD2*), for an enzyme involved in lipid modification (*UGT8*) and for molecules involved in the induction of apoptosis (*cytochrome c oxidase; COX6B1, Caspase9*). The results were consistent with preliminary observations from *in vitro* and *in vivo* studies and potentially explain the genetic mechanisms behind microbubble-induced damage to the vasculature as a new cancer therapy. They also reveal important bioeffects that ultrasound-stimulated microbubbles, alone and interacting with other forms of energy, can induce at a genetic level.

MATERIALS AND METHODS

Ultrasound treatments

Human umbilical vein endothelial cells (HUVEC) were obtained from American Type Culture Collection (ATCC; Manassas, VA, USA) and were cultured using an endothelial cell basal medium2 kit from Lonza (Walkersville, MD, USA). Cells were treated after three passages after trypsinization using 0.05% trypsine EDTA (GIBCO; Invitrogen, Carlsbad, CA, USA). A concentration of 2×10^6 cells/mL was used in each of the treatments that included subjecting the cells to radiation at 0 and 8 Gy using a CP160 cabinet xr-radiator system (Faxitron Xray Corporation, Lincolnshire, IL, USA) at 160 kVp energy and a dose rate of 200 cGy/minute. For microbubble-ultrasound treatments 3.3% (v/v) Definity microbubbles

(lipid-encapsulated perfluoropropane microbubbles, BristolMyers Squibb Medical Imaging, New York, NY, USA) (6×10^8 microbubbles) were added and exposed to 500-kHz ultrasound with 570-kPa peak negative pressure, which correspond to a mechanical index of 0.8 using a Valpey-Fisher transducer (Valpey-Fisher, Hopkinton, MA, USA). Cells were treated with a duty cycle of 10% for 30 s to avoid any potential heating and were constantly stirred to avoid effects of any potential lack of exposure to the ultrasound waves. Combined treatments were carried out by ultrasound exposure first and then irradiation of samples within 2 min. After treatment, cells were incubated at 37°C for up to 3 h and were then collected, and, nominally, 1 million cells were stored at 80°C for RNA analyses. The remaining cells were used in clonogenic (colony) assays *in vitro* to assess for treatment effects on cell survival. Some cells were plated for immunostaining and colorimetric assays.

Cells were treated with ultrasound in the presence of microbubbles (MB+US), radiation alone (8 Gy) or combined treatment (MB+US+8 Gy). Other experiments were indicated next used 2 Gy.

Isolation of RNA

Total RNA was isolated from HUVEC cells, which were treated as described before. Total RNA was isolated using Qiagen RNeasy Mini Kit according to the manufacturer's instructions (Qiagen, Mississauga, ON, Canada). The integrity of the RNA was confirmed using gel electrophoresis. Samples were then quantified using spectrophotometry.

Gene expression analyses

Microarray analyses. Human genome 28k microarray analysis was carried out at the SRI Genomics Core Facility at Sunnybrook Health Sciences Centre, ON, Canada. A human 28k genome of 70mer oligo probes was obtained from Qiage/Operon v2 (Qiagen) and the probes were immobilized onto epoxy-coated glass slides. Isolated RNA was used to derive complex cDNA probes, from which amino allyl-modified aRNA were synthesized. The aRNAs were coupled to Alexa 555 dye and were then hybridized to the 70mer whole-genome oligo microarrays. Microarray slides were blocked overnight at room temperature and rinsed five times with dH2O. A sample of 200 ng of each labeled aRNA was mixed with hybridization buffer (5x SSC and 0.1% SDS) and was then denatured at 95°C for 5 min. The final volume of 50 μL also contained 1% bovine serum albumin. The hybridization mix was then incubated on slides in a micorarray hybridization chamber at room temperature for 26 h. The slides were washed several times with 3x SSC/0.1% SDS and 1x SSC/0.1% SDS and then air dried.

Microarray chips were subsequently scanned by a Perkin Elmer Scan Array Express Scanner (Perkin Elmer, Waltham, MA, USA). The laser was set at 555 nm and the scan resolution was 10 microns. Images were quantified using Perkin Elmer QuantArray Software 3.0.1, and the intensities for each spot were estimated after background subtraction was carried out using the median intensity of the area surrounding each spot. Raw data were normalized and analyzed using Gene Spring software (Version 7.3.1; Agilent Technologies, Santa Clara, CA, USA). Normalization was performed using a per-chip 50th percentile method that normalized each chip based on its median values to permit comparison between chips. To highlight genes that characterize tissue, a per-gene on median normalization was performed. This normalized the expression of every gene by its median among samples. All samples were analyzed in duplicate. Original raw data and normalized data, as well as the data related to changes in expression, were all deposited in the MIAME (Minimum Information About a Microarray Experiment)–compliant public repository (Gene Expression Omnibus; GEO with accession number: GSE17525).

RT-PCR. To further validate elevated gene expression levels, RT-PCR was performed using a power SYBR green RNAtoCT 1step kit (Applied Biosystems, Foster City, CA, USA) according to the manufacturer's recommendations for quantification experiments on a RT-PCR system (7000 System). A set of primers was designed targeting genes related to membrane metabolism, lipid modifications and apoptosis that were upregulated as indicated by the microarray results. These genes included *MAP2K1*, *SMPD1*, *SMPD2*, *Caspase 9*, *COX6B1* and *UGT8*, and *β-actin* was used as an internal control gene. The sequences for all the primers are listed in Table 1 and were synthesized by Integrated DNA Technologies (IDT, Coralville, IA, USA). The RNA was reverse-transcribed at a hold cycle at 48°C for 30 min, which was followed by the PCR amplification as a one-step run. The cycling parameters for the PCR were: holding at 95°C for 10 min followed by 40 cycles, which included denaturing at 95°C for 15 s and annealing/extension at 53°C for 1 min. The RT-PCR was performed using an ABI Prism 7000 System (Applied Biosystems) and data were analyzed using ABI Prism 7000 Sequence Detection System (SDS) Version 1.0 Software (Applied Biosystems). The cycle thresholds (Ct) from triplicates for most samples were used to access the level of expression. The replicated Ct values for different samples were compared with those of the control values after normalization to the internal control gene values. This was done using the $2^{-\Delta\Delta Ct}$ method as was previously described (Schmittgen and Livak 2008; Peirson et al. 2003) as a relative approach

Table 1. Sequences (5′ to 3′) of the primers used in the detection of the different genes

Gene	Forward	Reverse
MAP2K1	ATCGTGGGCTTCTATGGT	GTCTTTCTGGCGACATGT
UGT8	GACCAGAGTACAGGCAAAAG	CCAGGTTGATCCTTGTGA
SMPD2	AGCTCCCCAACCATGAA	CTGCCAATGATTCCGCT
SMPD1	ATCGGCCTTAATCCTGGT	AGCCCATAGGTTTCTCGA
Caspase 9α	TGTGAACTTCTGCCGTGA	AGCTCCAGCAAAGCCA
Caspase 9β	CGAAGCCAACCCTAGAAAAC	GCCACCTCAAACCCATG
COX6B1	CCTTTAGGATTCAGCACCATG	AGATGCAGCCAGTTCAGA
Beta Actin	CCAGCACAATGAAGATCAAGA	ACTCGTCATACTCCTGCT

used to determine the change in gene expression level relative to other samples (Schmittgen and Livak 2008). Statistical analyses were carried out using (GraphPad Prism 4, GraphPad Software Inc., La Jolla, CA, USA); the Mann-Whitney *U* test or *t*-tests were used. *p*-values ≤ 0.05 indicated significance.

Clonogenic assays and immunohistochemistry. After treatments with or without sphingosine-1-phosphate (SPP; Sigma Aldrich, St. Louis, MO, USA), 1.0×10^3 cells from the control, irradiation, ultrasound-activated microbubble-exposed and combination treatment samples (using 2-Gy radiation doses for survival assays) were plated in triplicate and incubated at 37°C in 5–10% CO_2 for a week to develop colonies.

Treatments with SPP were carried out with ultrasound exposure to test the role of ceramide in the response of endothelial cells to ultrasound-stimulated microbubble exposure. For experiments

Two-Gy radiation conditions were used as a control because very little ceramide is produced with that radiation dose, whereas at 8 Gy, all cells would die when given as one fraction, making rescue infeasible. Colonies were then fixed and stained with 0.3% methylene blue/methanol for 20 min. The numbers of the counted colonies were then compared and *t*-test was used to assess the statistical significance. In addition, cells were plated on glass coverslips in multiwell plates to give a monolayer of cells. Plates were kept in the 37°C incubator for up to 3 h. Cells were then fixed in 1% paraformaldehyde for 20 min at room temperature and were washed with phosphate-buffered saline (PBS). Immunostaining was then carried out using a Histostain-*Plus* kit (Invitrogen), following the manufacturer's instructions. Before staining, samples were permeabilized using 0.1% triton (Sigma Aldrich) in PBS for 20–30 min. A monoclonal ceramide antibody at a concentration of 20 g/mL was then used in the detection of ceramide (Alexis Biochemical, San Diego, CA, USA). The polyclonal UGT8 and SMPD1 antibodies were obtained from Abnova (Walnut, CA, USA) and were used at a dilution of 1:80. Cells were then imaged using a Leica DM LB light microscope and Leica IM1000 software (Leica, Wetzlar, Germany).

Colorimetric assays to quantify ceramide. After treatments, cells were plated into 12-well plates and incubated in a 37°C incubator for up to 3 h. Cells were then fixed in 1% paraformaldehyde for 20 min and were permeabilized with 0.1% triton X100 (Sigma Aldrich). After blocking for 1 h at room temperature with 3% bovine serum albumin (Sigma Aldrich), cells were incubated with anticeramide antibody (1:1000) for another hour at room temperature. Extensive washes in PBS were performed and were followed by 1-h incubation with the horseradish peroxidase–conjugated secondary antibody (1:2000, Amersham, Quebec, Canada). After more washes, 1 mL of oPhenylenediamine dihydrochloride (OPD) substrate (Sigma Aldrich) was added and incubated for 2 min. This was followed by adding 200 μL of 3N HCL to stop the reactions. We then used a spectrophotometer to read the optical density of the supernatant at a wavelength of 492 nm.

RESULTS

Gene expression up-regulation and ceramide involvement

Whole-genome array analyses were carried out to survey gene expression changes and to identify candidate genes for quantitative RT-PCR analyses. After evaluating RNA integrity (Fig. 1a), samples were subjected to microarray analysis. Microarray results identified 19,264 genes in the HUVEC cells and indicated an up-regulation of 239–517 genes, depending on the treatment, where the change in expression was more than two-fold. We were specifically interested in investigating responses to treatment that affects genes involved in apoptosis, as well as genes related to cell membrane metabolism because we used ultrasound-stimulated microbubbles to cause mechanical disturbances to the membranes of cells. This can result in cell stress or may even transiently damage the cell membrane. Sphingomyelin (SM) is a lipid associated with the cell membrane and is a substrate to both sphingomyelin phosphodiesterase 1 (acid lysosomal sphingomyelinase, *ASM, SMPD1*) and sphingomyelin phosphodiesterase 2 (neutral sphingomyelinase, *SMPD2*) enzymes, which, when stimulated, led to ceramide

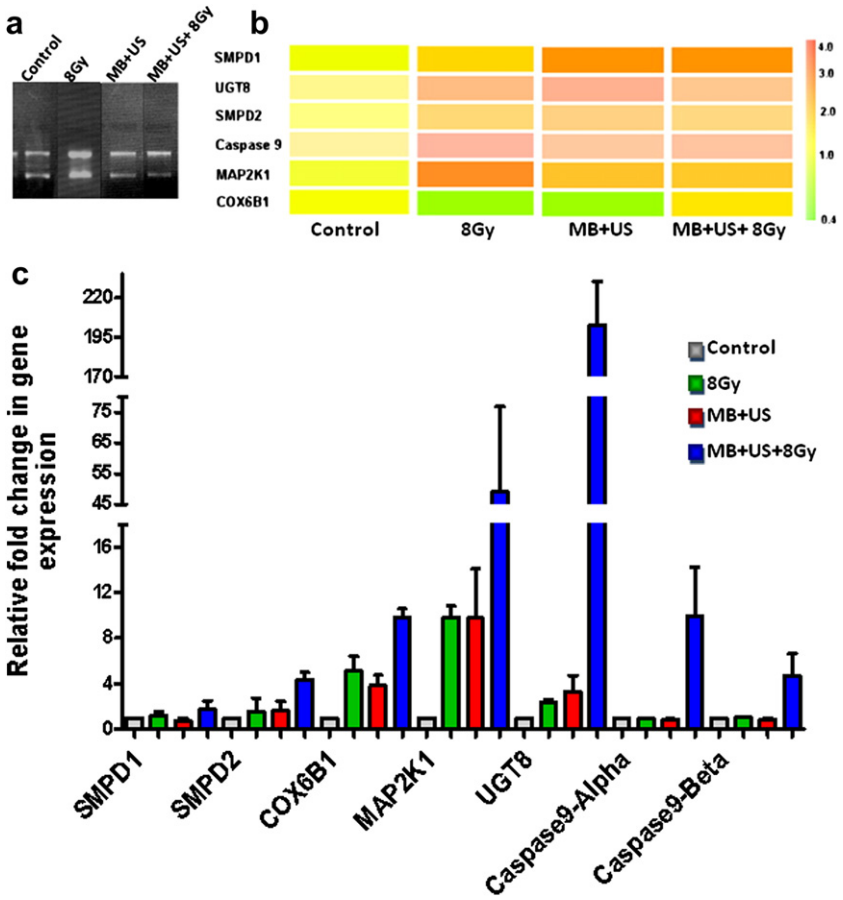

Fig. 1. Evaluations of levels of gene expression in HUVEC cell, under various conditions. (a) Gel electrophoresis of isolated RNA samples used in analyses (microarrays and RT-PCR) demonstrating RNA integrity. (b) Heat map illustrating a summary of the microarray change in levels of the indicated genes in samples treated with MB+US+8 Gy or MB+US or 8 Gy only. The change in color from yellow to pink indicates the strength of the signal. (c) Validation of gene expression data using RT-PCR. Delta delta Ct values were calculated in reference to those of *β-actin* and have indicated the different relative levels of gene expression in samples treated with either ultrasound-activated microbubbles, US+MB+8Gy or 8 Gy only. The *p*-values and level of significance were calculated using the Mann-Whitney *U* test or *t*-test (Table S2).

production. The corresponding genes were selected for analysis on this basis.

The gene expression levels for these two enzymes were elevated to a very minor level in combined treatments with a relative increase of 1.96 ± 0.13 for *SMPD1* ($p < 0.04$) but less so (1.6 ± 0.06, $p < 0.04$) for *SMPD2* (Fig. 1b, Table S1). Single treatment with ultrasound and microbubbles, or radiation (8 Gy) alone, did not result in increases in the expression of these genes. Because any resulting ceramide production could increase the permeability of the mitochondria, resulting in the release of cytochrome c, we checked for related gene expression changes. An elevated level of the *cytochrome c oxidase* (*COX6B1*) gene was also observed with combined treatments with a 1.8 ± 1.4–fold increase (Fig. 1b). Cytochrome c is an important molecule involved in the formation of the apoptosome complex, essential for the activation of caspase 9, and hence we also examined its gene. The expression level of the gene that encodes for caspase 9 was also observed to be elevated in the combined treatment samples with a 3.4 ± 1.4–fold increase (Fig. 1b, Fig. S1). Caspase 9 can activate other caspases, such as caspase 3, which would lead to the initiation of apoptosis. Another pathway that may also lead to apoptosis can involve UDP glycosyltransferase 8 (UDPgalactose ceramide galactosyltransferase [UGT8]), and enzyme known to be involved in the formation of galactosylceramide, a key molecule involved in cellular pathways that would lead to apoptosis (Fig. 4). The *UGT8* gene was also observed to be elevated by 2.6 ± 0.36–fold in the combined ultrasound and radiation treatment (Fig. 1b, Fig. S1) but had a *p*-value of < 0.07. We also investigated mitogen-activated protein kinase kinase 1 (MAP2K1), which is another protein usually associated with cell proliferation, yet is involved in pathways that lead to apoptosis under

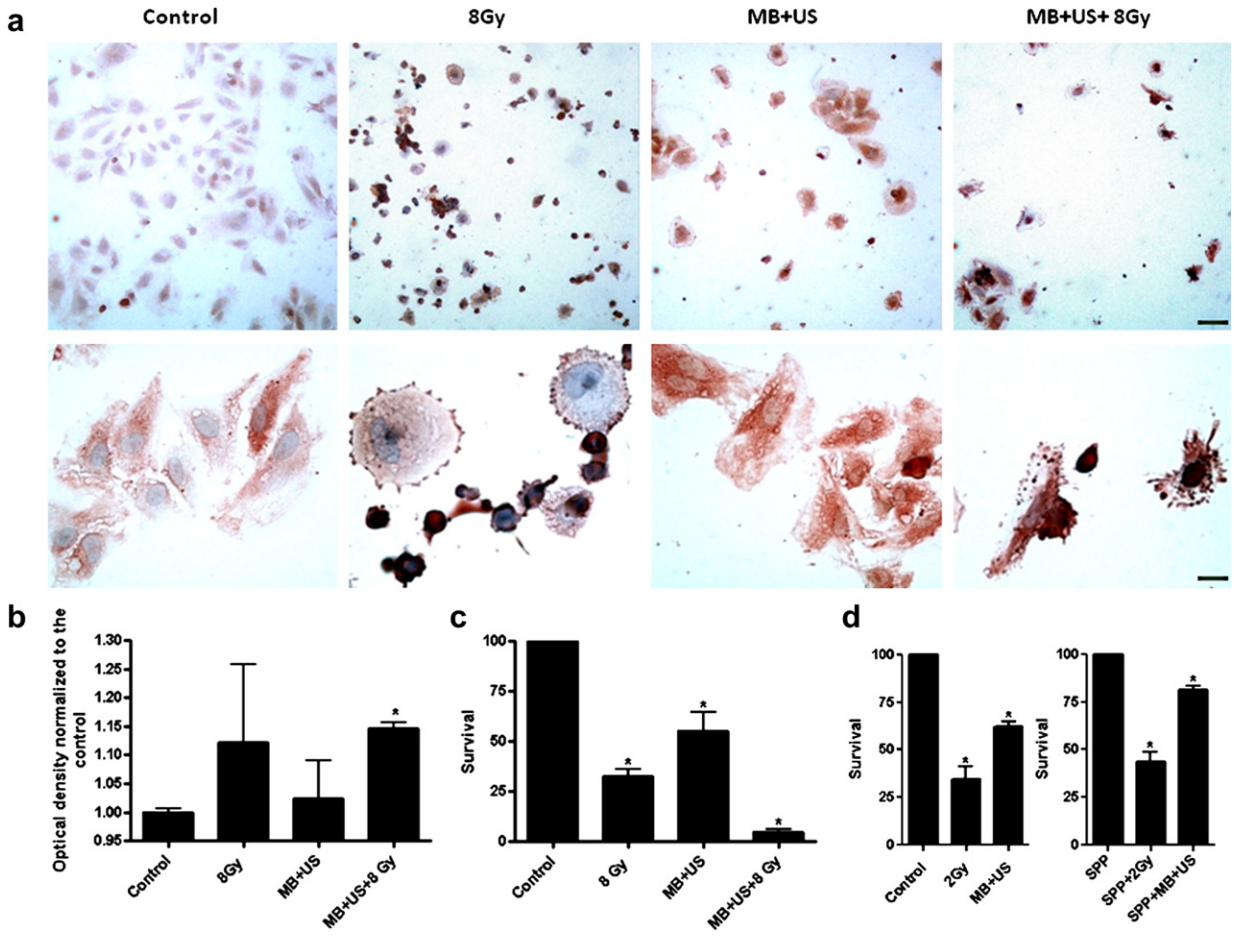

Fig. 2. Ceramide detection in HUVEC treated with different conditions. Immunohistochemical staining for ceramide: (a) upper panel showing micrographs at low magnification and lower panel showing micrographs at high magnification. The micrographs illustrate control, with light staining of an endogenous ceramide (control); treatments with 8 Gy only show intense ceramide staining in damaged cells (8 Gy); cells treated with ultrasound-stimulated microbubbles (MB+US), illustrating a more intense staining; and cells subjected to combined treatment of MB+US+8 Gy undergo apoptosis and are associated with intense immunostaining for ceramide. (b) Colorimetric quantitation of ceramide revealed an increase in ceramide levels under the various treatments when compared with the control. (c) Evaluations of cell death under different conditions using clonogenic assays indicated a cell death of 45% ($p < 0.0195$) for cells treated with ultrasound-activated microbubbles, 67% ($p < 0.0014$) for cells treated with 8 Gy only and 95% ($p < 0.0002$) for cells subjected to the combined treatments. (d) The use of SPP inhibited the ceramide activity through the observed enhancement of cell survival under the therapeutic conditions, which included radiation alone or ultrasound-activated microbubbles. SPP+2Gy showed statistically significant difference compared with SPP+MB+US ($p \leq 0.05$, *t*-test). The scale bar for the upper panel represents 50 μm and for the lower panel represents 25 μm. *Statistically significant results compared with the control sample.

extreme stress conditions. Its gene was found to be elevated only a small amount at 1.4 ± 0.16–fold in the combined treatments (Fig. 1b, Fig. S1) and had a *p*-value that was not significant. Statistical analyses were carried out using the T-test and Mann-Whitney *U* test and are summarized in Table S1.

Quantitative analyses of the candidate genes indentified from gene array analyses were undertaken. Because the microarray approach relies on the hybridization of oligonucleotides to cRNA targets determining the relative abundance of gene copies based on the intensity of the fluorescence, a validation approach was used to support the microarray results using RT-PCR. RT-PCR results were evaluated using the Ct method to indicate the relative ratio of the gene level in the treated samples *versus* that in the control after normalization to the expression levels of *β-actin* gene, a "housekeeping" gene. Increases in the relative levels of genes were observed specifically with the combined treatments, with Ct values of 4.3 ± 0 .69 for *SMPD2* ($p \leq 0.05$), 9.82 ± 0.76 for *COX6B1* ($p \leq 0.05$), 9.98 ± 4.3 for *caspase 9α* ($p \leq 0.05$) and 4.67 ± 1.97 for *caspase 9β* ($p \leq 0.5$) (Fig. 1c, Table S2). The change of 1.73 ± 0.76 for *SMPD1* was not significant with a $p \leq 0.35$.

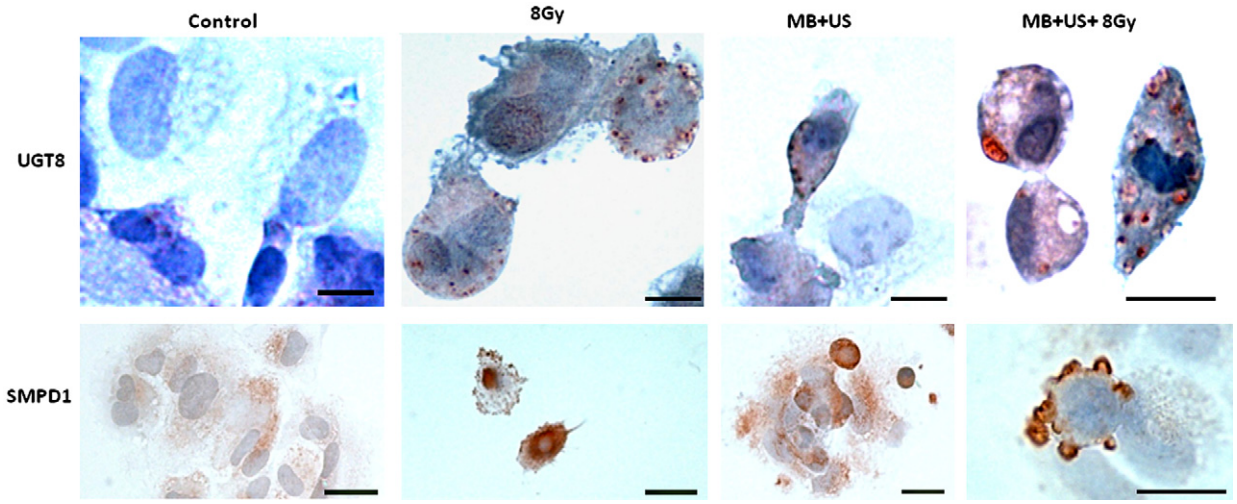

Fig. 3. Apoptotic morphology and associated detection of *UGT8* and *SMPD1* using immunohistochemistry. *(Top row)* Detection of *UGT8*: (control) untreated control cells, (8 Gy) cells subjected to either 8 Gy only; or (US+MB) cells treated with ultrasound-activated microbubbles show specific reactivity in damaged cells; or to (US+MB+8Gy) a combined treatment of 8 Gy and ultrasound-activated microbubbles resulted in cellular damage, leading to apoptotic morphologies and demonstrating immunostaining of UGT8 in specific compartments throughout the cells. Scale bars represent 15 μm. Detection of SMPD1 (panels as for UGT8). Scale bars for control, 8 Gy, MB+US represent 25 μm, and 12 μm for MB+US+8 Gy.

As for UGT8 and MAP2K1, which follow different signaling pathways that could also lead to apoptosis, up-regulation was also observed with a Ct value of 202 $\pm$ 27.5 for *UGT8* and 49.05 $\pm$ 27.8 for *MAP2K1* (both with $p \leq 0.05$). For the single-microbubble and ultrasound- or radiation-alone treatments, the Ct values were lower (Fig. 1c, Table S2), with insignificant changes in several genes that otherwise for the combined treatment had a $p \leq 0.05$. For instance, for ultrasound-stimulated microbubble treatment, only *COX6B1* and *MAP2K1* and *UGT8* were significantly increased. For 8 Gy, only MAP2K1 and UGT8 were statistically significantly increased, with $p \leq 0.04$.

To test the functional significance of ceramide production in response to ultrasound-activated microbubbles treatments, endothelial cells were treated with ultrasound in the presence and absence of microbubbles, with and without 1 μM SPP, which inhibits ceramide effects on cells. Results, presented in Figure 3, indicated a preservation of cell viability in the presence of SPP with a 19.4% $\pm$ 1.4 ($p \leq 0.0011$) elevation in the relative protection of surviving cells when treatments with ultrasound-activated microbubbles were conducted in the presence of SPP.

Experiments and analyses here were conducted using a HUVEC cell suspension model, cell survival assessments and ceramide immunohistochemistry. An opticell cell-growth measure was also used and found to be similar in regards to colony-assay cell survival, (Fig. 2c, Fig. 3SE) in response to the treatments. However, for gene analyses only the suspension model was used to provide adequate genetic materials because the opticell method uses cell monolayer with a small exposure area and would have limited the amount of RNA needed for gene array analyses.

Ceramide detection and the effect of treatments

A ceramide monoclonal antibody was used to characterize response to treatment in terms of ceramide. Immunostaining indicated an increased ceramide production in response to treatment with microbubbles in the presence of ultrasound (Fig. 2a) when compared with the control (Fig. 2a). A similar increase was observed when cells were treated with either a combination of bubbles in the presence of ultrasound and radiation or 8 Gy alone (Fig. 2a).

We also evaluated the levels of ceramide in cells subjected to different treatment conditions, using colorimetric assays, and found the ceramide levels to be elevated in all the conditions when compared with the control. However, this was only significant when comparing the combined treatment with that of the control ($p < 0.0268$) (Fig. 2b). Nevertheless, cell morphology was different for the different samples with more diffuse staining with treatment with microbubbles and ultrasound, and more intense staining with apoptotic morphology with the combined treatments.

Some of the cells from each of the different conditions were not fixed but rather were used for colony assays. Plated cells were allowed to grow forming colonies, which were then fixed and counted. The numbers of colonies were then normalized to those of the control. A 45% ($p < 0.0195$) cell death was observed with microbubble treatment in the presence of ultrasound,

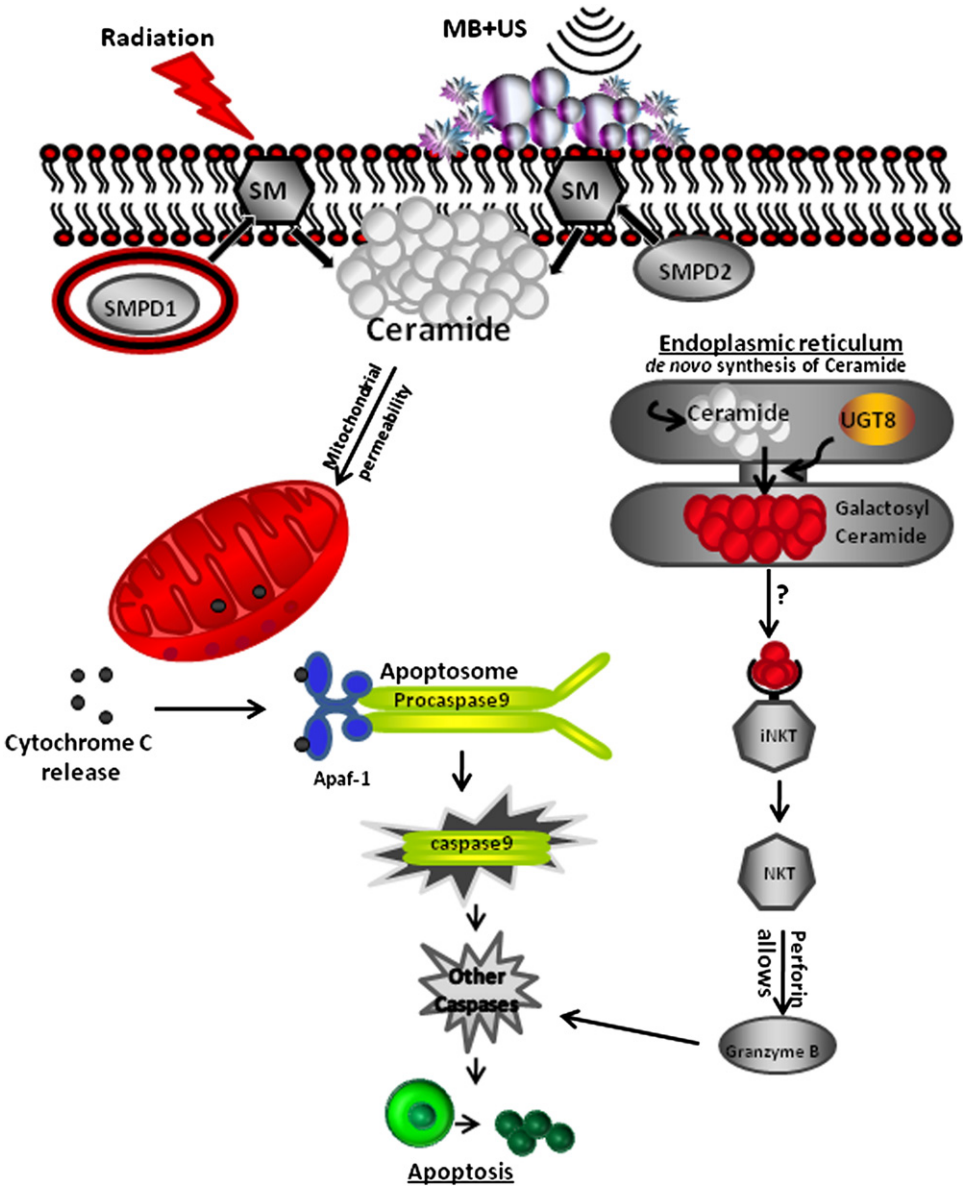

Fig. 4. A proposed schematic model of apoptotic mechanistic pathways in HUVEC based on gene expression changes in the combined treatments using microbubbles, ultrasound and X-ray radiation. The putative hydrolysis of sphingomyelin (SM) by the sphingomyelinases (SMPD1 and SMPD2) results in the production of ceramide, which can act on mitochondria to facilitate the release of cytochrome c. This could then complex with procaspase 9 and Apaf1. The formed complex (apoptosome) in the presence of ATP leads to the activation of caspase 9, which can then activate other caspases and can ultimately initiate apoptosis. Alternatively, ceramide produced from *de novo* synthesis in the endoplasmic reticulum can be modified by UGT8 to form galactosyl-ceramide, which is a molecule known to activate the iNKT cells. Active NKT cells will then secrete perforin, which assembles at the target cell plasma membrane and allows the passage of granzyme B, leading to apoptotic pathways.

67% ($p < 0.0014$) with 8 Gy only and 95% ($p < 0.0002$) with the combined treatments (Fig. 2c). Our experiments further indicated the importance of ceramide production because inhibition of its effects with SPP led to a preservation of endothelial cells viability with ultrasound exposure in the presence of microbubbles (Fig. 2d). Data are presented as mean ± SEM, and statistical analyses were carried out using the Mann-Whitney *U* test or *t*-test.

Cell morphology and the specific detection of UGT8 and SMPD1 in apoptotic cells

Treated cells exhibited classic apoptotic morphology (Fig. 3). To verify *UGT8* up-regulation, we conducted immunohistochemistry to ascertain the presence of the gene product and its localization. This appeared to be localized within a granular distribution (Fig. 3). This observation was mainly restricted to damaged cells

undergoing apoptosis with obvious changes in cellular structure. The increased numbers of apoptotic cells were observed in cells treated with either microbubbles in the presence of ultrasound, 8 Gy radiation only or a combination of both (Fig. 3) treatments. In addition, immunolabeling of the SMPD1 enzyme illustrated changed staining pattern localized at the membranes of the apoptotic cells (Fig. 3).

DISCUSSION

Microbubbles have been identified to induce bioeffects at physiologic and tissue levels. Such effects can under ultrasound condition different from those used in this study and can be a result of an increase in temperature caused by the bubble oscillation (Hilgenfeldt et al. 2000). Other effects on cellular membranes include an increased influx of ions through membrane ion channels and lead to the polarization of cellular membranes (Juffermans et al. 2008). In addition, it has been reported that ultrasound-stimulated microbubbles can induce the production of free radicals (Takahashi et al. 2007), which can be damaging and induce cell death. Other applications relying on ultrasound modulation of biology have included drug and gene delivery as cancer therapies, where targeted microbubbles were used as delivery vehicles (Korpanty et al. 2007; Yan et al. 2011). However, an exact mechanism of action of microbubbles at a molecular level has yet to be understood. We have recently developed an ultrasound-microbubble approach targeting xenograft tumors in mice to enhance radiation effects that leads to high levels of endothelial cell apoptosis and vascular disruption when used with radiation in tumors. To our knowledge, this is the first analysis of their anticancer effect at a gene expression level in a well-controlled cell culture system focusing on their effect on blood vessel–lining endothelial cells. This is the cell type that such bubbles would interact with *in vivo*.

Microarray technology was used to identify candidate genes that changed with treatments. Quantification through RT-PCR was then carried out on these candidates. There was an expected difference between the results from the two technologies. Because the microarray approach is based on the hybridization of the sample RNA to a gene chip, the level of sensitivity is relatively poor compared with more quantitative methods. Yet, it enables the screening of a very large pool of genes in one analysis. Results need to be validated by another more precise approach, such as quantitative RT-PCR (Canales et al. 2006; Zou et al. 2002; VanGuilder et al. 2008). Although RT-PCR is a more sensitive approach, because it is based on the specific amplification of the sequence of the gene(s) of interest, only a few genes can be analyzed simultaneously. This explains why in the cases of *MAP2K1* and *UGT8*, the PCR data analyses demonstrated a much greater change compared with the microarray technology. In addition, the immunolabeling of UGT8 enzyme (Fig. 3) also illustrated changes in UGT8 protein cellular location specifically under the combined treatments of ultrasound-stimulated microbubbles and 8 Gy (Fig. 3). Although *SMPD1* expression was not increased, similar changes in cellular distribution occurred, which may be involved in a stress or cell repair response.

Exposure to ultrasound-stimulated microbubbles in this study led to changes in gene expression. Key genes identified by microarray analysis that were up-regulated in HUVEC cells by exposure to microbubbles in the presence of ultrasound included: *SMPD2*, which is a membrane-bound enzyme related to membrane damage signaling, exhibiting less significant changes in gene expression; *COX6B1* and *MAP2K1*, which are genes related to downstream cell death signaling that were elevated in expression further; other genes are involved in lipid biogenesis and repair such as *UGT8* that were also found to be elevated; and *caspase 9* genes that were elevated in the combination treatments but not in the treatments with single modalities consistent with apoptosis induction. Immunohistochemistry indicated the production of ceramide in response to microbubble exposure and, in particular, significantly different-appearing staining in response to ultrasound-stimulated microbubble exposure when combined with radiation.

Overall, these genes code for proteins believed to be involved in the ceramide-regulated cell death pathways in response to microbubbles and ultrasound exposure. To validate these results we used a common approach, RT-PCR, which is a sensitive, precise method to evaluate gene expression (VanGuilder et al. 2008; Canales et al. 2006). This approach further demonstrated much higher relative gene expression levels, specifically with the ultrasound-microbubble treatments when radiation was added.

More specifically, the genes *SMPD1* and *SMPD2* are believed to hydrolyze sphingomyelin to produce ceramide, which is involved in apoptosis as was previously reported (GarciaBarros et al. 2003; Sánchez et al. 2007). We did not find significant increases in *SMPD1*, only in *SMPD2*. However, the intracellular location of *SMPD1* did exhibit changes in treatments involving microbubbles and ultrasound with staining at the cell membrane.

Ceramide was identified using immunohistochemistry and colorimetric assays in treated samples, where elevated levels were noticed. The colorimetric assays were used as an additional validation method that showed a significant increase in ceramide levels comparing the control with the combined treatment. Immunohistochemistry demonstrated different patterns of ceramide staining

for the cells with more intense staining with the combined treatment and cell blebbing. In contrast, more diffuse staining was seen with ultrasound-stimulated microbubbles.

However, the exact pathway of ceramide production and the mechanism determining cell death has been debated (Green 2000; Tepper et al. 2000; Barnes 2004), proposing an apoptotic pathway that does not involve the mitochondria or the nucleus in Jurkat T cells. Nevertheless, research conducted using HUVEC cells has indicated the involvement of ceramide in the production of reactive oxygen species from the mitochondria (Corda et al. 2001). Additional research reviews suggest that ceramide can be generated by multiple pathways—in the plasma membrane, in the lysosomes by SMPD1, *de novo* in the endoplasmic reticulum or by SMPD2 in the mitochondria. Any of these pathways may lead to apoptosis (Ogretmen and Hannun 2004).

In the ultrasound and microbubble treatments here, ceramide is likely produced in response to cell membrane damage. This could be direct physical damage caused by active cavitation or microstreaming and jets produced by passive cavitation. Alternatively, chemical damage formed by lipid peroxidation caused by free radicals that can potentially be formed in surrounding media with bubble collapse (Takahashi et al. 2007) can also potentially cause membrane damage. In addition, it has been demonstrated that ceramide in mitochondria leads to the release of cytochrome c, which acts as a cofactor and is aided by Apaf1 (apoptotic peptidase activating factor 1) in the assembly of the apoptosome, a caspase9 activating complex. Activated caspase 9 is then involved in a proteolytic cascade to activate other caspases, eventually leading to cell death (Acehan et al. 2002; Hill et al. 2003). Alternatively, *de novo* ceramide has been suggested to directly regulate the alternative splicing of caspase 9b in lung adenocarcinoma cells (Chalfant et al. 2002). A model pathway of these interactions is presented in Figure 4.

Our results indicated an up-regulation of the sphingomyelinase genes *SMPD2*, in addition to *cytochrome c oxidase* (COX6B1) and *caspase 9*, which seems to support the involvement of an apoptotic pathway involving the mitochondria. This up-regulation was more evident when radiation was combined with ultrasound-microbubble exposure. Although there is little statistical data supporting the elevation of *SMPD1* levels, the protein's spatial distribution has changed (immunolabeling; Fig. 3). Other pathways as illustrated in the model figure (Fig. 4) may be involved because we also observed a notable elevation in the *ceramide galactosyltransferase* (*UGT 8*) gene in response to the combined treatment. This could be related to membrane biogenesis occurring during repair of the endothelial cells as suggested by immunohistochemistry. The protein product of *UGT8* is an integrated protein of the membrane of the endoplasmic reticulum that converts the ceramide to galactosylceramide and is used as a marker in cancer prognosis (Ruckhäberle et al. 2009; Dziecedil Giel et al. 2010). The metabolite galactosylceramide (alphagalactosylceramide), which was originally extracted from a marine sponge, is a potent activator of invariant natural killer T (iNKT) cells (Kronenberg 2004; Wilson and Delovitch 2003; Vincent et al. 2003). The activated NKT cells were reported to release cytotoxic granules, such as perforin and granzymes, to induce apoptotic cell death through pathways that can either include the activation of caspases or may be caspase-independent (Lieberman 2003). However, it has been reported that the hydrolysis of galactosylceramide leads to the production of ceramide as well (Ogretmen and Hannun 2004). Whether the elevated levels of the *UGT8* gene, which we have observed in the combined treatment, can lead to cell death through any of these pathways or lead to the production of more ceramide, is a question that needs to be addressed in future research. Alternatively, ceramide produced from *de novo* synthesis in the endoplasmic reticulum can be modified by UDP-galactose ceramide galactosyltransferase (UGT8) to form galactosyl-ceramide, which is a molecule known to be involved in apoptotic pathways.

Radiation combined with ultrasound-stimulated microbubbles induced changes in gene expression levels, leading to the activation of ceramide apoptotic pathway. Previous reports have indicated that the use of ionized radiation alone induces the up-regulation of genes associated with the DNA damage cycle, leading to apoptosis (Ayoub et al. 2008; Bao et al. 2006). Such genes include; *p53*, *GADD45A*, *H2AX*, *BTG1&2* and *XPC*, which were not up-regulated in this study in response to microbubble exposure in the presence of ultrasound. In addition, the gene for checkpoint kinase 1 (CHEK1), which mediates cell cycle arrest signaling in response to DNA damage, was also not up-regulated. Yet our results indicated some up-regulation of genes that code for DNA ligase 1 and XRCC5, known to be involved in DNA repair (Prasad et al. 2010; Moeller et al. 2011).

External effectors at the cell membrane such as low linear energy transfer (LET) γ radiation have also been reported to activate the sphingomyelin pathway at the cell membrane, independent of DNA damage, to produce ceramide, which leads to apoptosis (Seideman et al. 2011).

The experiments here were carried out using cells suspended *in vitro* to ensure uniformity of interactions with cell membranes. The effect induced is potentially more pronounced compared with a system where adherent cells are used; however, experiments we have conducted using opticell as a cell carrier have yielded similar cell responses in terms of cell survival (Fig. S3), which could be a result of the heightened sensitivity of HUVEC cells.

Gene expression levels could be different in adherent cells, although any effects of trypsinization and detaching cells should be controlled for as gene array results are compared with trypsinized and detached control cells.

In this study we have exposed cells to a physical therapy: microbubbles in the presence of ultrasound, which act to damage the cell membrane. We then investigated the potential mechanism of bioeffect action through the evaluation of the differential gene expression levels discussed here. The resulting expressed proteins are involved in lipid/cell membrane metabolism (SMPD2 and UGT8) and can also lead to ceramide production activating cell death. Both radiation alone and ultrasound-activated microbubbles acted to activate similar genes, but to a greater extent when used together, coinciding with an observed synergy when these conditions are combined *in vivo* (Czarnota et al., 2012; Tran et al., 2012). Cell morphology, in addition to immunohistochemistry of UGT8 and SMPD1 location, was suggestive of gene-product accumulation at sites of microbubble-induced deformities in cell membranes.

We have demonstrated an ultrasound-induced bioeffect in which key genes involved in ceramide-induced apoptotic pathways are activated after ultrasound exposure in the treatment with microbubbles. We have also functionally demonstrated here an important role for ceramide because an inhibitor of ceramide-reduced cell death resulted in enhanced survival of endothelial cells after microbubble exposure in the presence of ultrasound. Ceramide has been reported to date to be produced in different cellular compartments that include membrane lipid rafts, lysosomes, mitochondria and endoplasmic reticulum and can be metabolized in the Golgi apparatus (Ogretmen and Hannun 2004). Ceramide and its metabolites are involved in many pathways, some leading to apoptosis.

The knowledge of the key genes involved in this new therapy of using ultrasound and microbubbles to sensitize cells potentially through the production of ceramide is important. Knowledge of the genetic pathways involved should permit an optimization of response and provides insight into the mechanism of action of microbubble effects on endothelial cells. The research here forms a basis to developing anticancer therapy based on the use of microbubbles and ultrasound as an enhancer of radiation effect further. The research also reveals important bioeffects that ultrasound-stimulated microbubbles can induce at a genetic level, which can interact with effects from other forms of energy.

Acknowledgments—This work was supported by the CCSRI, NSERC, and the Terry Fox Foundation. GJC is supported by a CCO Research Chair in Experimental Therapeutics and Imaging in addition to Clinician Scientist Funding from the Ontario Ministry of Health and Long Term Care. We thank the Department of Radiation Oncology and Sunnybrook Health Sciences Centre for infrastructure support.

SUPPLEMENTARY DATA

Supplementary data related to this article can be found online at http://dx.doi.org/10.1016/j.ultrasmedbio.2012.07.009

REFERENCES

Acehan D, Jiang X, Morgan DG, Heuser JE, Wang X, Akey CW. Three dimensional structure of the apoptosome: Implications for assembly, procaspase9 binding, and activation. Mol Cell 2002;9:423–432.

Alonso A, Dempfle CE, Della Martina A, Stroick M, Fatar M, Zohsel K, Allémann E, Hennerici MG, Meairs S. In vivo clot lysis of human thrombus with intravenous abciximab immunobubbles and ultrasound. Thromb Res 2009;124:70–74.

Ayoub N, Jeyasekharan AD, Bernal JA, Venkitaraman AR. HP1-beta mobilization promotes chromatin changes that initiate the DNA damage response. Nature 2008;29:682–686.

Bao S, Wu Q, McLendon RE, Hao Y, Shi Q, Hjelmeland AB, Dewhirst MW, Bigner DD, Rich JN. Glioma stem cells promote radioresistance by preferential activation of the DNA damage response. Nature 2006;444:756–760.

Barnes PJ. Ceramide lances the lungs. Nat Med 2004;10:130–131.

Bautch VL. Endothelial cells form a phalanx to block tumor metastasis. Cell 2009;136:810–812.

Bergers G, Hanahan D. Modes of resistance to anti-angiogenic therapy. Nat Rev Cancer 2008;8:592–603.

Brown AT, Flores R, Hamilton E, Roberson PK, Borrelli MJ, Culp WC. Microbubbles improve sonothrombolysis in vitro and decrease hemorrhage in vivo in a rabbit stroke model. Invest Radiol 2011; 46:202–207.

Canales RD, Luo Y, Willey JC, Austermiller B, Barbacioru CC, Boysen C, Hunkapiller K, Jensen RV, Knight CR, Lee KY, Ma Y, Maqsodi B, Papallo A, Peters EH, Poulter K, Ruppel PL, Samaha RR, Shi L, Yang W, Zhang L, Goodsaid FM. Evaluation of DNA microarray results with quantitative gene expression platforms. Nat Biotechnol 2006;24:1115–1122.

Chalfant CE, Rathman K, Pinkerman RL, Wood RE, Obeid LM, Ogretmen B, Hannun YA. De novo ceramide regulates the alternative splicing of caspase 9 and Bclx in A549 lung adenocarcinoma cells. J Biol Chem 2002;277:12587–12595.

Chopra R, Vykhodtseva N, Hynynen K. Influence of exposure time and pressure amplitude on blood-brain-barrier opening using transcranial ultrasound exposures. ACS Chem Neurosci 2010;1:391–398.

Corda S, Laplace C, Vicaut E, Duranteau J. Rapid reactive oxygen species production by mitochondria in endothelial cells exposed to tumor necrosis factor is mediated by ceramide. Am J Respir Cell Mol Biol 2001;24:762–768.

Czarnota CJ, Karshafian R, Burns PN, Wong S, Al Mahrouki A, Lee J, Caissie A, Tran W, Kim C, Furukawa M, Wong E, Giles A. Ultrasound induced microbubble enhancement of tumor radiation response. Proc Natl Acad Sci U S A 2012;109:E2033-41.

Dziecedil Giel P, Owczarek T, Plazuk E, Gomułkiewicz A, Majchrzak M, Podhorska-Okołów M, Driouch K, Lidereau R, Ugorski M. Ceramide galactosyltransferase (UGT8) is a molecular marker of breast cancer malignancy and lung metastases. Br J Cancer 2010;103:524–531.

Ellis LM, Hicklin DJ. VEGF targeted therapy: Mechanisms of antitumour activity. Nat Rev Cancer 2008a;8:579–591.

Ellis LM, Hicklin DJ. Pathways mediating resistance to vascular endothelial growth factor targeted therapy. Clin Cancer Res 2008b;14: 6371–6375.

French D, Flannery R, Groetsch C, Krantz W, Kleene S. Numerical approximation of solutions of a nonlinear inverse problem arising in olfaction experimentation. Math Comput Model 2006;43: 945–956.

GarciaBarros M, Paris F, CordonCardo C, Lyden D, Rafii S, Haimovitz-Friedman A, Fuks Z, Kolesnick R. Tumor response to radiotherapy regulated by endothelial cell apoptosis. Science 2003;300:1155–1159.

Gerst S, Hann LE, Li D, Gonen M, Tickoo S, Sohn MJ, Russo P. Evaluation of renal masses with contrast-enhanced ultrasound: Initial experience. AJR Am J Roentgenol 2011;197:897–906.

Green DR. Apoptosis and sphingomyelin hydrolysis: The flip side. J Cell Biol 2000;150:F5–F7.

Hanahan D, Folkman J. Patterns and emerging mechanisms of the angiogenic switch during tumorigenesis. Cell 1996;86:353–364.

Hilgenfeldt S, Lohse D, Zomack M. Sound scattering and localized heat deposition of pulse-driven microbubbles. J Acoust Soc Am 2000; 107:3530–3539.

Hill MM, Adrain C, Martin SJ. Portrait of a killer: The mitochondrial apoptosome emerges from the shadows. Mol Interv 2003;3:1926.

Hoyt K, Sorace A, Saini R. Quantitative mapping of tumor vascularity using volumetric contrast-enhanced ultrasound. Invest Radiol 2011 [Epub ahead of print].

Hu G, Liu C, Liao Y, Yang L, Huang R, Wu J, Xie J, Bundhoo K, Liu Y, Bin J. Ultrasound molecular imaging of arterial thrombi with novel microbubbles modified by cyclic RGD in vitro and in vivo. Thromb Haemost 2011 [Epub ahead of print].

Jalali S, Huang Y, Dumont DJ, Hynynen K. Focused ultrasound-mediated BB disruption is associated with an increase in activation of AKT: Experimental study in rats. BMC Neurol 2010;10:114.

Juffermans LJ, Kamp O, Dijkmans PA, Visser CA, Musters RJ. Low-intensity ultrasound-exposed microbubbles provoke local hyper polarization of the cell membrane via activation of BK(Ca) channels. Ultrasound Med Biol 2008;34:502–508.

Karshafian R, Samac S, Bevan PD, Burns PN. Microbubble mediated sonoporation of cells in suspension: Clonogenic viability and influence of molecular size on uptake. Ultrasonics 2010;50:691–697.

Klotz AR, Lindvere L, Stefanovic B, Hynynen K. Temperature change near microbubbles within a capillary network during focused ultrasound. Phys Med Biol 2010;55:1549–1561.

Korpanty G, Carbon JG, Grayburn PA, Fleming JB, Brekken RA. Monitoring response to anticancer therapy by targeting microbubbles to tumor vasculature. Clin Cancer Res 2007;13:323–330.

Kronenberg M. Presenting fats with SAPs. Nat Immunol 2004;5: 126–127.

Liao ZK, Tsai KC, Wang HT, Tseng SH, Deng WP, Chen WS, Hwang LH. Sonoporation-mediated anti-angiogenic gene transfer into muscle effectively regresses distant orthotopic tumors. Cancer Gene Ther 2012;19:171–180.

Lieberman J. The ABCs of granule mediated cytotoxicity: New weapons in the arsenal. Nat Rev Immunol 2003;3:361–370.

McDannold NJ, Vykhodtseva NI, Hynynen K. Microbubble contrast agent with focused ultrasound to create brain lesions at low power levels: MR imaging and histologic study in rabbits. Radiology 2006;241:95–106.

McDannold N, Zhang Y, Vykhodtseva N. Blood-brain barrier disruption and vascular damage induced by ultrasound bursts combined with microbubbles can be influenced by choice of anesthesia protocol. Ultrasound Med Biol 2011;37:1259–1270.

Mammoto A, Connor K, Mammoto T, Yung C, Huh D, Aderman C, Mostoslavsky G, Smith L, Ingber D. A mechanosensitive transcriptional mechanism that controls angiogenesis. Nature 2009;457: 1103–1108.

Moeller BJ, Yordy JS, Williams MD, Giri U, Raju U, Molkentine DP, Byers LA, Heymach JV, Story MD, Lee JJ, Sturgis EM, Weber RS, Garden AS, Ang KK, Schwartz DL. DNA repair biomarker profiling of head and neck cancer: Ku80 expression predicts locoregional failure and death following radiotherapy. Clin Cancer Res 2011;17:2035–2043.

Nikolova-Karakashian MN, Rozenova KA. Ceramide in stress response. Adv Exp Med Biol 2010;688:86–108.

Ogretmen B, Hannun YA. Biologically active Sphingolipids in cancer pathogenesis and treatment. Nat Rev Cancer 2004;4:604–616.

Olson P, Chu GC, Perry SR, Nolan-Stevaux O, Hanahan D. Imaging guided trials of the angiogenesis inhibitor sunitinib in mouse models predict efficacy in pancreatic neuroendocrine but not ductal carcinoma. Proc Natl Acad Sci U S A 2011;108:E1275–E1284.

O'Reilly MA, Huang Y, Hynynen K. The impact of standing wave effects on transcranial focused ultrasound disruption of the blood-brain barrier in a rat model. Phys Med Biol 2010;55:5251–5267.

Peirson SN, Butler JN, Foster RG. Experimental validation of novel and conventional approaches to quantitative real time PCR data analysis. Nucleic Acids Res 2003;31:e73.

Prasad R, Shock DD, Beard WA, Wilson SH. Substrate channeling in mammalian base excision repair pathways: Passing the baton. J Biol Chem 2010;285:40479–40488.

Ruckhäberle E, Karn T, Rody A, Hanker L, Gätje R, Metzler D, Holtrich U, Kaufmann M. Gene expression of ceramide kinase, galactosyl ceramide synthase and ganglioside GD3 synthase is associated with prognosis in breast cancer. J Cancer Res Clin Oncol 2009;135:1005–1013.

Rota C, Raeman CH, Child SZ, Dalecki D. Detection of acoustic cavitation in the heart with microbubble contrast agents in vivo: A mechanism for ultrasound-induced arrhythmias. J Acoust Soc Am 2006; 120:2958–2964.

Sánchez AM, MalagarieCazenave S, Olea N, Vara D, Chiloeches A, DíazLaviada I. Apoptosis induced by capsaicin in prostate PC3 cells involves ceramide accumulation, neutral sphingomyelinase, and JNK activation. Apoptosis 2007;12:2013–2024.

Schmittgen TD, Livak KJ. Analyzing real-time PCR data by the comparative C(T) method. Nat Protoc 2008;3:1101–1108.

Seideman JH, Stancevic B, Rotolo JA, McDevitt MR, Howell RW, Kolesnick RN, Scheinberg DA. Alpha particles induce apoptosis through the sphingomyelin pathway. Radiat Res 2011;176:434–446.

Sorace AG, Warram JM, Umphrey H, Hoyt K. Microbubble-mediated ultrasonic techniques for improved chemotherapeutic delivery in cancer. J Drug Target 2012;20:43–54.

Suchting S, Eichmann A. Jagged gives endothelial tip cells an edge. Cell 2009;137:988–990.

Takahashi M, Chiba K, Li P. Free-radical generation from collapsing microbubbles in the absence of a dynamic stimulus. J Phys Chem B 2007;111:1343–1347.

Tepper AD, Ruurs P, Wiedmer T, Sims PJ, Borst J, Blitterswijk WJV. Sphingomyelin hydrolysis to ceramide during the execution phase of apoptosis results from phospholipids scrambling and alters cell surface morphology. J Cell Biol 2000;150:15564.

Tozer GM, Kanthou C, Baguley BC. Disrupting tumour blood vessels. Nat Rev Cancer 2005;5:423–435.

Tran TA, Le Guennec JY, Babuty D, Bougnoux P, Tranquart F, Bouakaz A. On the mechanisms of ultrasound contrast agents-induced arrhythmias. Ultrasound Med Biol 2009;35:1050–1056.

Tran WT, Iradji S, Sofroni E, Giles A, Eddy D, Czarnota GJ. Microbubble and ultrasound radioenhancement of bladder cancer. Br J Cancer 2012;107:469–476.

VanGuilder HD, Vrana KE, Freeman WM. Twenty-five years of quantitative PCR for gene expression analysis. Biotechniques 2008;44: 619–626.

Vincent MS, Gumperz JE, Brenner MB. Understanding the function of CD1restricted T cells. Nat Immunol 2003;4:51723.

Wilson SB, Delovitch TL. Janus-like role of regulatory iNKT cells in autoimmune disease and tumour immunity. Nat Rev Immunol 2003;3:211–222.

Wood AK, Bunte RM, Price HE, Deitz MS, Tsai JH, Lee WM, Sehgal CM. The disruption of murine tumor neovasculature by low-intensity ultrasound-comparison between 1- and 3-MHz sonication frequencies. Acad Radiol 2008;15:1133–1141.

Yan F, Li X, Jin Q, Jiang C, Zhang Z, Ling T, Qiu B, Zheng H. Therapeutic ultrasonic microbubbles carrying paclitaxel and LyP-1 peptide: Preparation, characterization and application to ultrasound-assisted chemotherapy in breast cancer cells. Ultrasound Med Biol 2011;37:768–779.

Zou J, Young S, Zhu F, Gheyas F, Skeans S, Wan Y, Wang L, Ding W, Billah M, McClanahan T, Coffman RL, Egan R, Umland S. Microarray profile of differentially expressed genes in a monkey model of allergic asthma. Genome Biol 2002;3:research0020.